Frontiers of Information Technology & Electronic Engineering
www.jzus.zju.edu.cn; engineering.cae.cn; www.springerlink.com
ISSN 2095-9184 (print); ISSN 2095-9230 (online)
E-mail: jzus@zju.edu.cn

Improvement of signal processing in Coriolis mass flowmeters for gas-liquid two-phase flow*

Chunhui LI[†1], Lijun SUN[†‡1], Jiarong LIU[1], Yang ZHANG[1], Haiyang LI[2], Huaxiang WANG[1]

[1]*School of Electrical and Information Engineering, Tianjin University, Tianjin 300072, China*

[2]*Shanghai Institute of Measurement and Testing Technology, Shanghai 201203, China*

[†]E-mail: ChunhuiLi@tju.edu.cn; sunlijun@tju.edu.cn

Received Oct. 13, 2019; Revision accepted July 14, 2020; Crosschecked Sept. 7, 2020

Abstract: As an increasingly popular flow metering technology, Coriolis mass flowmeter exhibits high measurement accuracy under single-phase flow condition and is widely used in the industry. However, under complex flow conditions, such as two-phase flow, the measurement accuracy is greatly decreased due to various factors including improper signal processing methods. In this study, three digital signal processing methods—the quadrature demodulation (QD) method, Hilbert method, and sliding discrete time Fourier transform method—are analyzed for their applications in processing sensor signals and providing measurement results under gas-liquid two-phase flow condition. Based on the analysis, specific improvements are applied to each method to deal with the signals under two-phase flow condition. For simulation, sensor signals under single- and two-phase flow conditions are established using a random walk model. The phase difference tracking performances of these three methods are evaluated in the simulation. Based on the digital signal processor, a converter program is implemented on its evaluation board. The converter program is tested under single- and two-phase flow conditions. The improved signal processing methods are evaluated in terms of the measurement accuracy and complexity. The QD algorithm has the best performance under the single-phase flow condition. Under the two-phase flow condition, the QD algorithm performs a little better in terms of the indication error and repeatability than the improved Hilbert algorithm at 160, 250, and 420 kg/h flow points, whereas the Hilbert algorithm outperforms the QD algorithm at the 600 kg/h flow point.

Key words: Coriolis mass flowmeter; Digital signal processing method; Two-phase flow condition; Quadrature demodulation; Sliding discrete time Fourier transform (SDTFT); Hilbert transform

https://doi.org/10.1631/FITEE.1900558 **CLC number:** TH814

1 Introduction

Coriolis mass flowmeters are widely used in the industry because of their direct measurement of fluid mass flow and high measurement accuracy under the single-phase flow condition (Wang T and Baker, 2014). However, problems exist in Coriolis mass flowmeter applications in complex flow conditions, such as the gas-liquid two-phase flow condition. Under the two-phase flow condition, the resonance frequency of the measuring tube constantly fluctuates due to the change of the fluid density and the sharp increase of the damping ratio. The speed of traditional analog driving methods is relatively low, so the mass flow cannot be measured during the process of reconstructing the driving signal; this results in the loss of the measuring points and even the phenomenon in which the measuring tube oscillation ceases. Due to this problem, many scholars have proposed various digital signal processing methods to calculate the phase difference. These methods have achieved high accuracy under the single-phase flow condition. However, under the two-phase flow condition, the

‡ Corresponding author

* Project supported by the Scientific Research Project of Shanghai Municipal Bureau of Quality, China and the Technical Supervision Foundation of China (No. 2018-05)

ORCID: Chunhui LI, https://orcid.org/0000-0002-8854-2343; Lijun SUN, https://orcid.org/0000-0001-7547-2377

frequency and amplitude of the sensor signals fluctuate drastically, and the accuracies of different digital signal processing methods are affected to varying degrees.

Under the two-phase flow condition, liquid and gas have different densities. A terahertz (THz) imaging device for real-time multiphase flowmetering was proposed (Meribout et al., 2018, 2019). However, there is still no effective method for measuring two-phase flow using Coriolis flowmeters. When fluid flows in the measuring tube, the damping ratio of the measuring tube increases due to the dynamic characteristics of the gas-liquid two-phase flow; the amplitude of the signals from the measuring tube decreases, which causes errors in the measurement results (Tao et al., 2014). Due to the constant changes of the density of complex fluids, the damping ratio of the measuring tubes also changes continuously. Therefore, a driving system is required to track the change of the resonant frequency in time and change the output energy continually to maintain the vibration of the measuring tube.

The main ways to drive the measuring tube include analog drive and digital drive. Some scholars conducted a series of studies on analog drive and achieved certain results (Cage, 1988; Carpenter, 1988; Flecken, 1989; Kalotay et al., 1991).

Maginnis (2003) generated drive signals to drive and control the measuring tube using a multiplying digital-to-analog converter (MDAC). The sensor signal was connected to the analog input of the MDAC, and the processor adjusted the MDAC output gain according to the signals from sensors. Finally, the analog signal output by the MDAC passed through the operational amplifier to generate a drive signal to the driver. Huang et al. (2016) studied a new analog drive circuit to drive measuring tubes that abandon traditional methods, in which the circuit was composed of discrete components. Instead, the integrated chip technology was used to design the drive system, thus effectively avoiding interference problems caused by excessive discrete devices. Zamora and Henry (2008) developed a digital Coriolis converter using the combination of a Pentium processor and the field programmable gate array (FPGA). The digital signal method was adopted to process the underlying sensor signals, and a digitally driven method based on waveform synthesis was used to drive tube vibration in the system. The development of this digital system enables the measurement of more complex fluids, such as two-phase flow, but the cost of the Pentium processor is relatively high. Li XG and Xu (2009) proposed a driving scheme based on a nonlinear amplitude control algorithm, which not only shortened the starting time of the measuring tube but also strengthened control of the measuring tube drive under the two-phase flow condition. Li M et al. (2010) studied optimization of the driving method and used a random sequence and signal synthesis to maintain stable vibration of the measuring tube. A combination of a digital drive based on the phase-locked loop (PLL) principle and a traditional analog drive for drive control of the measuring tube was adopted by Shimada (2013).

The signal processing technology is the key to the Coriolis mass flowmeter and plays a decisive role in improving the accuracy and stability of Coriolis mass flowmeter measurement under different conditions. Because digital signal processing technology has experienced rapid development, many scholars have applied this technology to Coriolis mass flowmeter signal processing. The primary methods include quadrature demodulation (QD), the Hilbert transform, the discrete-time Fourier transform (DTFT), PLL, zero-crossing detection, the adaptive line enhancer (ALE), and the sliding Goertzel algorithm (SGA).

The QD method has been widely used to calculate the phase difference of sensor signals (Röck and Koschmieder, 2009; Wang JH, 2013; Kunze et al., 2014; Svete et al., 2015). Kunze et al. (2014) used the QD method for signal processing under the two-phase flow condition. However, the accuracy of the QD method is highly dependent on the design of the low-pass filter.

Yokoi and Owada (1996) used the Hilbert algorithm for signal processing of Coriolis mass flowmeters. Yang HY et al. (2012) proposed a new high-precision phase difference measurement method by combining the singular value decomposition (SVD) technique with the Hilbert algorithm. First, the signal was denoised by SVD and the original signal was reconstructed; then, the phase difference was calculated by the trigonometric function of the reconstructed signal and its Hilbert transform. Shen et al. (2017) proposed a new Coriolis flowmeter method to estimate the phase difference based on the correlation and Hilbert transform, and this method decreases the

influence of non-integral sampling and makes the algorithm more universal.

Romano (1990) used DTFT for signal processing of Coriolis mass flowmeters. Li Y et al. (2010) combined various filters with a negative frequency modified recursive algorithm to process signals of the Coriolis flowmeter. Shen et al. (2015) adopted the idea of sliding recursion based on the traditional DTFT algorithm, taking the influence of negative frequency components into account. However, due to the limitation of experimental conditions, the real-time phase difference and time difference were not obtained. The measured time difference was obtained according to the performance curve of the flowmeter.

Zhang et al. (2017) estimated the accuracy of measuring mass flow with a 15% density drop by simulation without real-time experimental calibration.

In summary, many scholars have proposed various converter designs and digital signal processing methods to address the converter and signal processing of Coriolis mass flowmeters. They have compared and analyzed the signal processing methods. However, their results have not been evaluated or optimized according to the performance of the algorithm under actual working conditions, and whether the optimal signal processing algorithm among these methods is suitable for different gas volume fraction (GVF) conditions has not been determined through experimental results under the actual gas-liquid two-phase flow condition. To enhance the on-site measurement performance of Coriolis mass flowmeters, experiments under actual working conditions need to be done.

Based on the previous achievements of our research (Liu et al., 2018), we analyze three popular signal processing methods: QD, discrete Fourier transform (DFT), and Hilbert transform. We improve the DFT algorithm in our study. Calculation and redundancy of the DFT are greatly reduced using the actual frequency from PLL. Dropout and finite impulse response (FIR) are implemented in the Hilbert transform, which eliminates the effects of the endpoint and improves its accuracy. In addition, we calibrate the QD and Hilbert algorithms under single- and two-phase flow conditions. None of these has ever been done in previous research. The all-digital Coriolis flowmeter converter is designed based on a digital signal processor (DSP), and the improved methods are implemented on the converter. Various aspects of the improved signal processing methods are evaluated, such as measurement accuracy and complexity.

2 Algorithm improvement and analysis

2.1 Simulated signals

The random walk model (Li M and Henry, 2016) is used in the simulation to generate time-varying sensor signals with randomly varying frequency, amplitude, and phase difference:

$$\begin{aligned}
&s_1(n)=A(n)\sin\left(\frac{2\pi nf(n)}{f_s}+\frac{\varphi(n)}{2}\right)+\sigma_{e_1}e_1(n),\\
&s_2(n)=A(n)\sin\left(\frac{2\pi nf(n)}{f_s}-\frac{\varphi(n)}{2}\right)+\sigma_{e_2}e_2(n),\\
&A(n)=A(n-1)+\sigma_A e_A(n),\\
&f(n)=f(n-1)+\sigma_f e_f(n),\\
&\varphi(n)=\varphi(n-1)+\sigma_\varphi e_\varphi(n),
\end{aligned} \tag{1}$$

where $s_1(n)$ and $s_2(n)$ are the simulated sensor signals, $A(n)$ the amplitude, $f(n)$ the frequency, and $\varphi(n)$ the phase difference. $e_1(n)$, $e_2(n)$, $e_A(n)$, $e_f(n)$, and $e_\varphi(n)$ are white noise without correlation between each other. Meanwhile, σ_{e_1}, σ_{e_2}, σ_A, σ_f, and σ_φ are the coefficients generated by multiplying the walk amplitudes and walk factors for the random noise. The initial apparent density drop values of 15% and 50% under the two-phase flow condition are

$$\begin{cases}
A(0)=60\%,\ f(0)=240\ \text{Hz},\ \varphi(0)=1.64^\circ,\\
f_s=16\ \text{kHz},\ \sigma_A=0.27,\ \sigma_f=0.04,\\
\sigma_\varphi=2.5\times10^{-5},\ \sigma_{e_1}=\sigma_{e_2}=10^{-4},
\end{cases} \tag{2}$$

$$\begin{cases}
A(0)=60\%,\ f(0)=240\ \text{Hz},\ \varphi(0)=0.57^\circ,\\
f_s=16\ \text{kHz},\ \sigma_A=0.27,\ \sigma_f=0.08,\\
\sigma_\varphi=3.0\times10^{-5},\ \sigma_{e_1}=\sigma_{e_2}=10^{-4}.
\end{cases} \tag{3}$$

2.2 Quadrature demodulation

QD is a widely used technique to track the phase difference between two signals (Mehendale, 2008; Röck and Koschmieder, 2009; Kunze et al., 2014; Svete et al., 2015). It was also applied on the two-phase flow condition (Kunze et al., 2014).

Because filter design plays an important role in the accuracy of QD, in this study, we improve this method by further optimizing the filter structure and parameters. Considering the computational complexity and real-time performance of DSP, the infinite impulse response (IIR) digital filter is chosen for the low-pass filtering of the QD algorithm.

When the filter is in the k^{th} sampling, the input is $u(k)$ and output is $y(k)$. Then the filter calculates its output according to Eq. (4):

$$y(k)=\mathrm{LP_A}y(k-1)+\mathrm{LP_B}u(k), \tag{4}$$

where $\mathrm{LP_A}$ and $\mathrm{LP_B}$ are two coefficients of the filter, and $y(k-1)$ is the sample output at the $(k-1)^{\text{th}}$ sampling. $\mathrm{LP_A}$ and $\mathrm{LP_B}$ can be calculated as

$$\mathrm{LP_A}=f_s/(f_s+2\pi f_c), \tag{5}$$
$$\mathrm{LP_B}=1-\mathrm{LP_A}, \tag{6}$$

where f_s is the sampling frequency of the signal and f_c the cut-off frequency of the filter. When the signal with frequency higher than f_c passes through the filter, the signal amplitude greatly decreases and the signal with lower frequency maintains a certain amplitude.

f_c affects the computation accuracy of the algorithm. When f_c is high, the filter delay is relatively low, the filter output is sensitive to the noise, and the corresponding phase difference fluctuates. When f_c is low, the filter delay becomes large, the filter output is relatively stable, and the fluctuation of the phase difference can be dramatically reduced. MATLAB is used to simulate the QD method with different low-pass filter parameters under single- and two-phase flow conditions. Then, we evaluate their performances and select the low-pass filter with the best parameters.

The above-mentioned QD method needs to filter the original signal of double frequency and reserve the DC signal. Eqs. (7) and (8) show the process:

$$\frac{A_2}{2}\left[\cos\varphi_2-\cos(4\pi f_1 t+\varphi_2)\right]\Rightarrow \text{low-pass filter} \Rightarrow \frac{A_2}{2}\cos\varphi_2, \tag{7}$$

$$\frac{A_2}{2}\left[\sin\varphi_2+\sin(4\pi f_1 t+\varphi_2)\right]\Rightarrow \text{low-pass filter} \Rightarrow \frac{A_2}{2}\sin\varphi_2. \tag{8}$$

Two filter schemes, which are composed of six independent IIR low-pass filters, are compared in the test. For the convenience of description, they are numbered $\mathrm{LP_1}$–$\mathrm{LP_6}$. The first four filters, $\mathrm{LP_1}$–$\mathrm{LP_4}$, have the same coefficient. Their cut-off frequency is $f_{c1}=0.5f_1$ (Here, f_1 is the frequency of the sensor signal). The cut-off frequency of filters $\mathrm{LP_5}$ and $\mathrm{LP_6}$ in scheme 1 is $f_{c2}=0.005f_1$, and the cut-off frequency of filters $\mathrm{LP_5}$ and $\mathrm{LP_6}$ in scheme 2 is $f_{c2}'=0.45f_1$.

The random walk model (Röck and Koschmieder, 2009) is used to simulate time-varying sensor signals under single- and two-phase flow conditions. The sampling frequency f_s is 16 000 Hz. The number of sampled points is 80 000. The accuracy of the QD algorithm using two filtering schemes is evaluated by the root mean square error (RMSE):

$$\mathrm{RMSE}=\sqrt{\frac{1}{n}\sum_{i=1}^{n}\left(\hat{X}_i-X_i\right)_2}, \tag{9}$$

where $\hat{X}_i$ is the calculated phase difference, X_i the true value of the phase difference, and n the total number of calculation times. Accuracy of QD calculations is shown in Table 1.

Table 1 Accuracy of quadrature demodulation calculations

Condition	RMSE (°)	
	Scheme 1	Scheme 2
Single-phase flow	8.1520×10^{-5}	7.9288×10^{-4}
Two-phase flow	7.5648×10^{-3}	2.1886×10^{-2}

Compared with scheme 2, a lower cut-off frequency is implemented in scheme 1. Under single- and two-phase flow conditions, the RMSE of the phase difference results is smaller and the accuracy is higher. Thus, the parameters in scheme 1 are adopted for further experiments.

2.3 Hilbert transform

The method based on the Hilbert transform has been applied in Coriolis signal processing (Yokoi and Owada, 1996). For the endpoint effect phenomenon, the "dropout" method is adopted to discard the data at the endpoints on both sides of the signal; only the middle part is reserved for the calculation of the subsequent phase difference (Yang JW and Jia, 2006). For the original signal and the signal after the Hilbert

transform, the first 1/8 and the last 1/8 sampling points in a cycle are discarded, and the middle 3/4 sampling points are reserved for subsequent phase difference calculation. The random walk model is used to create signals of single- and two-phase flow in MATLAB. The signal-to-noise ratio (SNR) is set to 57 dB. Table 2 shows the RMSE values of the phase difference calculated using the Hilbert algorithm without or with dropout under single- and two-phase flow conditions.

Table 2 Accuracy of the Hilbert algorithm with or without dropout

Condition	RMSE (°)	
	Single-phase flow	Two-phase flow
Without dropout	8.0721×10^{-2}	1.8733×10^{-1}
With dropout	8.0329×10^{-2}	8.0580×10^{-2}

From the above results, the algorithm under the two-phase flow condition is much more influenced by the endpoint effect than under the single-phase flow condition due to the large fluctuation of the signal frequency and amplitude. The dropout technique can significantly weaken the influence of the endpoint effect on the results under the two-phase flow condition and improve the accuracy of the algorithm.

In addition, the Hilbert algorithm is more sensitive to noise. In the process of algorithm implementation, SNR significantly influences algorithm accuracy. In this study, the FIR sliding average filtering method is adopted in the Hilbert algorithm to improve accuracy.

The FIR moving average filter is the most commonly used filter in the time domain (Fan, 1995), and is optimal for suppressing random noise and preserving steep edges. Random noise causes erroneous measurement results. By means of multipoint aggregation and averaging, which can eliminate the influence of random noise to a maximum extent, reasonable data is obtained. The FIR moving average filter is expressed as

$$y(k)=\frac{1}{N}\sum_{i=0}^{N-1}x(k+i). \tag{10}$$

FIR performs filtering by convolving the input signal with a rectangular pulse. The larger the length of the moving average filter, the better the suppression performance of the random noise. The FIR sliding filter is applied after the Hilbert algorithm. The phase difference calculated by the algorithm is subject to moving average filtering. We change the length of the FIR filter and investigate the filtering effect of the FIR sliding average filter on the phase difference of the Hilbert algorithm.

The random walk model is used to create signals of single- and two-phase flow. The dropout technique is applied to the algorithm, and the 1/8 data of the front and rear endpoints is discarded. The ability to calculate the phase difference using the Hilbert algorithm with different FIR filter lengths is evaluated. FIR filter lengths are set to 1, 10, 100, and 1000. SNR is 57 dB. Figs. 1 and 2 show the phase difference results using the Hilbert algorithm with different FIR filter lengths under single- and two-phase flow conditions, respectively.

Tables 3 and 4 show the RMSE of the phase difference calculated by the Hilbert algorithm using FIR filters of different lengths under single- and two-phase flow conditions, respectively. It can be seen from the results that with the increase of the FIR filter length, the RMSE of the phase difference calculated by the Hilbert algorithm decreases. We can improve the accuracy of the algorithm by increasing the length of the FIR filter appropriately while meeting real-time requirements.

Table 3 Accuracy of the Hilbert algorithm with different FIR filter lengths under the single-phase flow condition

Length of the FIR filter	RMSE (°)
1	8.0174×10^{-2}
10	3.5353×10^{-2}
100	1.1654×10^{-2}
1000	3.5354×10^{-3}

Table 4 Accuracy of the Hilbert algorithm with different FIR filter lengths under the two-phase flow condition

Length of the FIR filter	RMSE (°)
1	8.1210×10^{-2}
10	3.5567×10^{-2}
100	1.1221×10^{-2}
1000	5.1398×10^{-3}

2.4 Discrete Fourier transform

Romano (1990) introduced DFT into Coriolis signal processing. In recent years, many scholars have studied the DFT method and proposed different

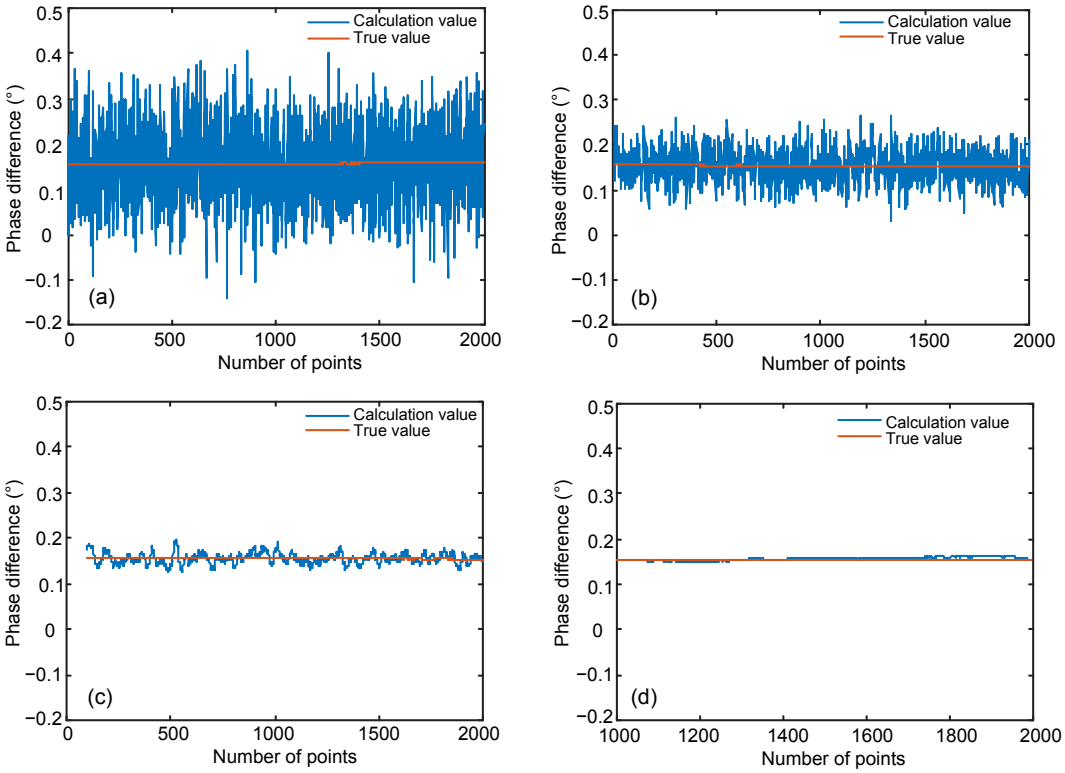

Fig. 1 Results of the Hilbert algorithm with the FIR filter lengths of 1 (a), 10 (b), 100 (c), and 1000 (d) under the single-phase flow condition (References to color refer to the online version of this figure)

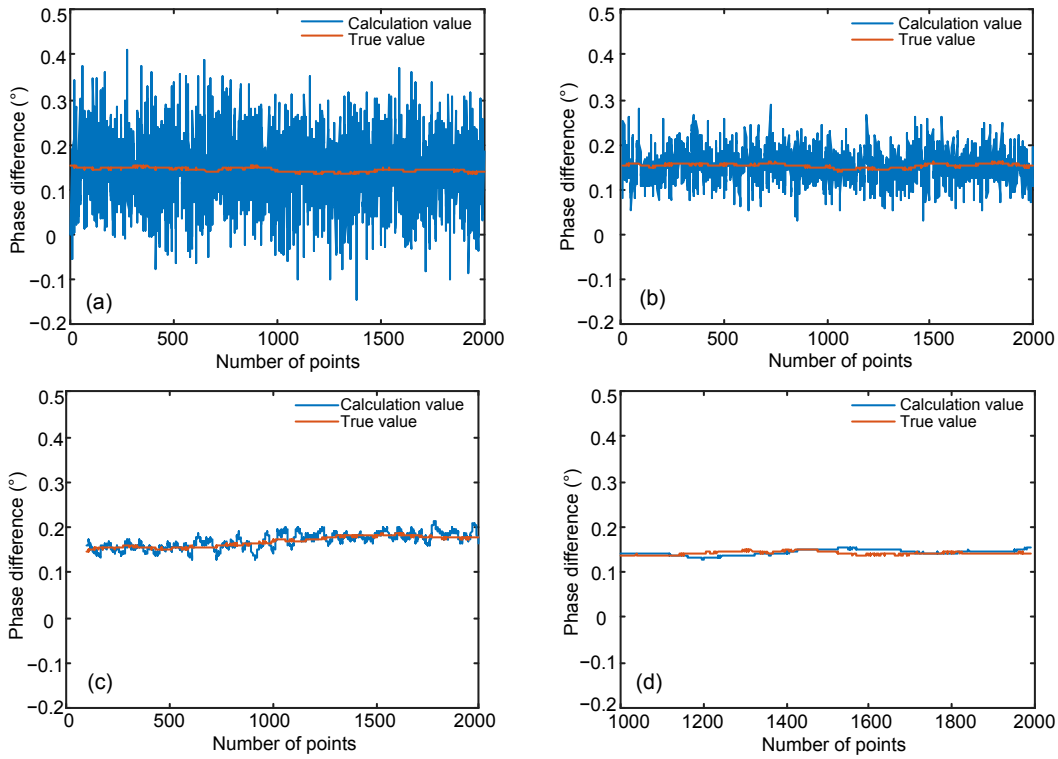

Fig. 2 Results of the Hilbert algorithm with the FIR filter lengths of 1 (a), 10 (b), 100 (c), and 1000 (d) under the two-phase flow condition (References to color refer to the online version of this figure)

measures to improve the DFT method, such as sliding DFT, recursive DTFT, and recursive sliding DTFT (SDTFT) (Tu and Zhang, 2008; Zhang et al., 2017).

The signal frequency is calculated by DFT, while the phase of the signal is obtained in the location of the maximum spectrum lines. The phase difference can be calculated by subtracting the phase of two signals.

This method is efficient in operation and resists the harmonic interference well. However, it needs integral period sampling and has a higher computational cost, which limits its practicality. When the sample sequence is not an integer multiple of the signal period, the spectral leakage problem results in phase difference errors (Tu and Zhang, 2008).

In this study, the traditional DFT is improved and the SDTFT which can greatly reduce the computational load of the algorithm is obtained. The traditional DFT is expressed as follows:

$$S_k = \sum_{n=0}^{N-1} s(n)\exp\left(-\frac{2\pi i}{N}kn\right),\ k=0,1,\ldots,N-1, \quad (11)$$

where $s(n)$ represents the original signal sampling sequence and S_k the DFT value under the frequency of kf_s/N. Eq. (11) can be expanded as follows:

$$S_k=\sum_{n=0}^{N-1} s(n)\left[\cos\left(\frac{2\pi kn}{N}\right)-i\sin\left(\frac{2\pi kn}{N}\right)\right], \quad (12)$$

where k=0, 1, …, N−1.

DFT is actually the correlation between the original signal and the sine and cosine signals of frequency kf_s/N, where k=0, 1, …, N−1. When k is a certain value, kf_s/N is closest to the signal frequency at which the signal obtains its peak value. The traditional DFT method uses the DFT value S_k at the frequency of kf_s/N to obtain the signal phase information. In the SDTFT algorithm designed in this study, the real frequency of the signal is substituted for kf_s/N, and the real frequency of the signal is obtained by the PLL of the driving part. Therefore, SDTFT is expressed as follows:

$$S_f = \sum_{n=0}^{N-1} s(n)\left[\cos\left(\frac{2\pi fn}{f_s}\right)-i\sin\left(\frac{2\pi fn}{f_s}\right)\right], \quad (13)$$

where f is the signal frequency obtained from the PLL, f_s the sampling frequency, and S_f the value after DFT of the signal at frequency f. When calculating the above formula, the length of the Fourier transform sequence is set to 4000, and the sliding method is used to update the DFT value every time a new sample point $s(n)$ is acquired. When n≤4000, the value of the new DFT is

$$S_{f,n} = S_{f,n-1} + s(n)\left[\cos\left(\frac{2\pi fn}{f_s}\right)-i\sin\left(\frac{2\pi fn}{f_s}\right)\right], \quad (14)$$

where S_{fn-1} is the value of the DFT at the last sampling point. When n>4000, DFT can be expressed as

$$\begin{aligned} S_{f,n} &= S_{f,n-1} \\ &- s(n-4000)\left[\cos\left(\frac{2\pi fn}{f_s}\right)-i\sin\left(\frac{2\pi f(n-4000)}{f_s}\right)\right] \\ &+ s(n)\left[\cos\left(\frac{2\pi fn}{f_s}\right)-i\sin\left(\frac{2\pi fn}{f_s}\right)\right]. \end{aligned} \quad (15)$$

Thus, the phase of the original signal is

$$\arg(S_f) = \operatorname{atan}\left(2(\operatorname{Im}(S_f),\operatorname{Re}(S_f))\right), \quad (16)$$

where Im refers to the imaginary part of a complex number, and it forms a complex number with the real part referred to as Re.

The phase difference can be obtained by subtracting the phase of two signals. The SDTFT designed in this study obtains the real frequency of the signal through the PLL, to directly calculate the DFT at the real frequency of the signal. Furthermore, the calculation cost of the traditional DFT algorithm is greatly reduced by adopting the sliding method.

3 Comparison of algorithms

To verify the anti-noise performance of SDTFT, we compare the SDTFT algorithm with the QD and Hilbert algorithms. The random walk model is used to establish the sensor signal under the single-phase flow condition, and the random noise (white noise) of different SNRs is added to the signal to evaluate the

accuracy of the phase difference between these three algorithms. As shown in Fig. 3, the SNRs of the signals are set to 37, 57, and 77 dB. The three algorithms are evaluated in these three cases because SNR values can reflect the real situation to a great extent. Table 5 shows the RMSE of the phase difference results.

According to Fig. 3 and Table 5, the QD and Hilbert algorithms are more sensitive to noise. As the SNR decreases, the accuracy of the QD and Hilbert algorithms decreases by 1–2 orders of magnitude. The accuracy of the SDTFT algorithm is almost unaffected by the SNR. It has good anti-noise performance.

Under the single-phase flow condition, the frequency and amplitude of signals are relatively stable. The SDTFT algorithm has a small error and high

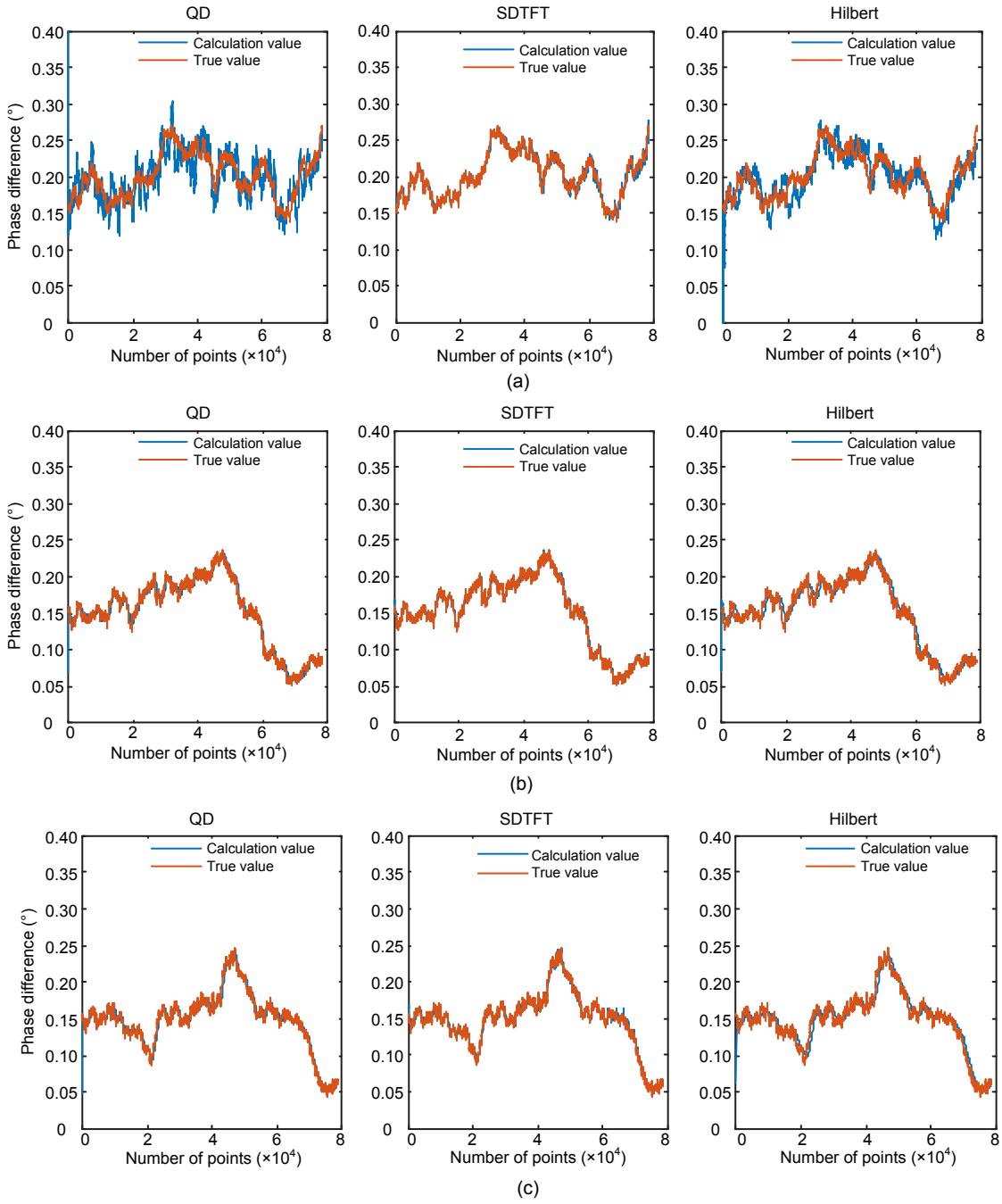

Fig. 3 Results of the QD, SDTFT, and Hilbert algorithms with different signal-to-noise ratios (SNRs) under the single-phase flow condition: (a) SNR=37 dB; (b) SNR=57 dB; (c) SNR=77 dB

precision. Under the two-phase flow condition, the frequency and amplitude of signals fluctuate greatly. To evaluate the accuracy of the SDTFT algorithm under the two-phase flow condition, the random walk model is used to establish the sensor signals under single- and two-phase flow conditions. We set the sampling frequency f_s to 1000 Hz, the number of sampling points N to 80 000, and SNR to 57 dB. Figs. 4 and 5 show the phase difference results of the three algorithms under single- and two-phase flow conditions, respectively. Table 6 shows the RMSE of the calculation results. Table 7 shows the computation time results of these three algorithms.

Table 5 Indication error of the phase difference obtained using the three algorithms

Algorithm	RMSE (°)		
	SNR=37 dB	57 dB	77 dB
QD	2.2137×10^{-2}	2.4907×10^{-3}	1.4036×10^{-3}
SDTFT	8.1123×10^{-4}	7.4495×10^{-4}	8.3253×10^{-4}
Hilbert	2.1360×10^{-2}	2.1257×10^{-3}	8.0486×10^{-4}

From Table 7, the computation time of the QD algorithm is the shortest, while that of the Hilbert algorithm is the longest. From the point of view of accuracy, under the single-phase flow condition, all these three algorithms can track the phase difference of the calculated signals. RMSEs of the QD and Hilbert algorithms are slightly larger than that of the

Table 6 Errors of the three algorithms in phase difference calculation

Algorithm	RMSE (°)	
	Single-phase flow	Two-phase flow
QD	2.6553×10^{-3}	1.0713×10^{-2}
SDTFT	7.7421×10^{-4}	2.1986×10^{-1}
Hilbert	2.1798×10^{-3}	6.8203×10^{-3}

Table 7 Computation time of the three algorithms

Algorithm	Computation time (s)
QD	0.296 844
SDTFT	0.417 790
Hilbert	1.520 965

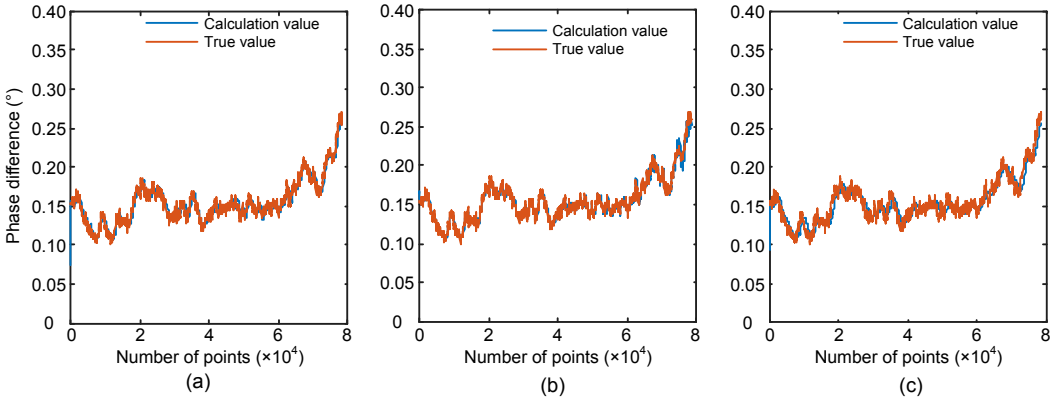

Fig. 4 Phase difference results obtained using the QD (a), SDTFT (b), and Hilbert (c) algorithms under the single-phase flow condition (References to color refer to the online version of this figure)

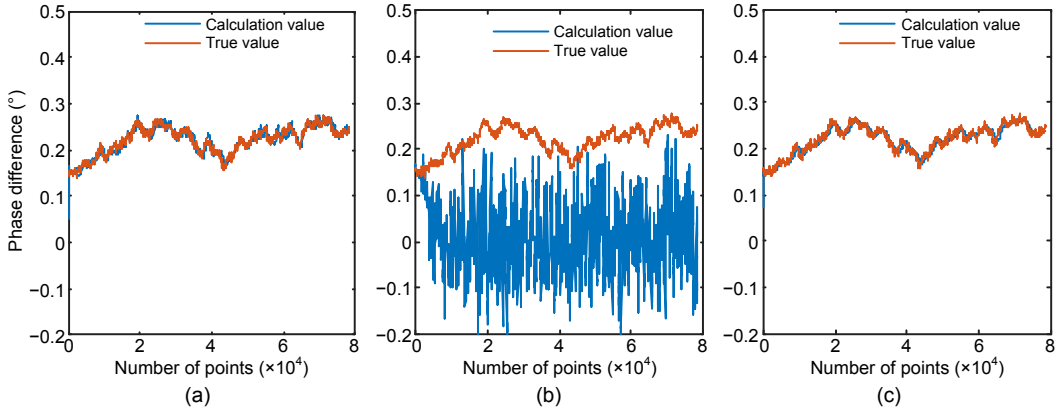

Fig. 5 Phase difference results obtained using the QD (a), SDTFT (b), and Hilbert (c) algorithms under the two-phase flow condition (References to color refer to the online version of this figure)

SDTFT algorithm. Under the two-phase flow condition, the accuracies of the QD and Hilbert algorithms are reduced, and the phase difference can be tracked. However, the SDTFT algorithm cannot track the phase difference due to the large frequency fluctuation under the two-phase flow condition.

4 Experimental verification

4.1 Converter design

Algorithms were implemented on an embedded platform. The converter system implemented three major functions, i.e., digital driving, digital signal processing, and universal serial bus (USB) communication. One button was used to select whether to implement the QD algorithm or not. The software system is shown in Fig. 6.

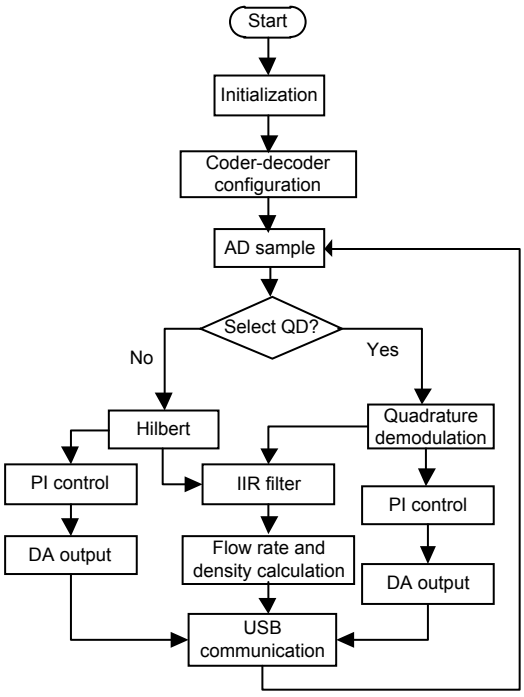

Fig. 6 Software system of the Coriolis mass flowmeter converter
AD: analog-to-digital; QD: quadrature demodulation; DA: digital-to-analog; IIR: infinite impulse response; PI: proportion integration; USB: universal serial bus

A digital driving method was implemented to drive the flow tube of the Coriolis flowmeter. The selected algorithm was executed to calculate the amplitude and phase, and the frequency and amplitude of the driving signal were controlled. The amplitude of the driving signal was adjusted through a proportion integration (PI) controller so that the flow tube vibrated at the set amplitude. The frequency control was based on the PLL. The PI controller was used to continuously adjust the frequency of the driving signal, which makes the phase difference between the sensor signal and the driving signal be zero. The reconstructed driving signal was output to the driver through the DA to actuate the oscillation of the flow tubes. These two algorithms were robust to frequency fluctuation and could track phase difference changes under the two-phase flow condition. Because the SDTFT algorithm is sensitive to frequency fluctuation, it was not adopted. The USB communication protocol was used to transmit information with the host computer. At the same time, this part can accept control commands and parameter modification from the host computer.

4.2 Experimental results

The digital driving method was experimentally verified under single- and two-phase flow conditions. The static start-stop gravitational method was used on the water flow rig to undertake calibration and testing based on the QD and Hilbert algorithms under single- and two-phase flow conditions.

4.2.1 Experiments under the single-phase flow condition

To verify the universality of the designed converter driving system, two different Coriolis mass flowmeter sensors were tested. The first sensor had twin bent tubes with an 8-mm inner diameter and the second sensor had twin bent tubes with a 25-mm inner diameter. Experiments were completed on the water flow rig (Fig. 7).

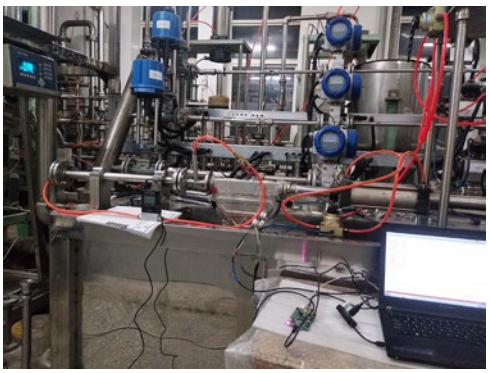

Fig. 7 A photo of the water flow rig

A start-stop method was adopted in our experiments. The standard calibration rig can achieve an expanded uncertainty of 0.03% (k=2). The gas flowmeter used in the experiments was an Alicat M series digital mass flowmeter (20-1-00-0-1000-600-KM2022, Alicat, USA) with a maximum flow rate of 600 mL/min. The maximum accuracy was 0.4% and repeatability was 0.2%. We took the value of the weighing scale as a reference and compared it with the accumulated flow obtained by the prototype converter using a digital signal processing (DSP). Each flow point was measured three times. Fluid density, driving signal frequency, driving signal amplitude, amplitude of the sensor signal, frequency of the sensor signal, and sensor signal phase information were obtained in a DSP. This information was uploaded to the personal computer (PC); the prototype converter could accept instruction from the PC and change the parameter at the same time.

The host computer collected the frequency and amplitude of the driving signal and the amplitude and phase information of the two signals from the sensors. Tables 8 and 9 show the average experimental data of two different sensors in 20 s under the single-phase flow condition. Among them, the 100% full-scale driving signal amplitude corresponded to a 1.3-V voltage, and the 100% full-scale sensor signal corresponded to a 212-mV voltage (150 mV RMS).

The phase value in Tables 8 and 9 is the average of the phase values from sensors A and B. This data was used as the input of the PI controlled phase for driving the module's PLL. In Table 8, for the 8-mm twin bent tubes, the repeatability of the converter driving process to frequency control was 0.000 75%. The sensor amplitude set value was about 40%, and the values of the repeatability of the amplitude control from two sensors were 0.149 72% and 0.107 00%. The average value of the PLL for the phase was 0.001 324 55° (set value was 0°), and the standard deviation was 0.027 55°. In Table 9, for the 25-mm twin bent tubes, the repeatability of the converter driving process to frequency control was 0.000 29%. The program amplitude set value was about 80%, and the values of the repeatability of amplitude control from two sensors were 0.021 98% and 0.020 18%. The average value of the PLL for the phase was 0.000 022 45° (set value was 0°), and the standard deviation was 0.010 53°.

4.2.2 Experiments under the two-phase flow condition

To evaluate the driving effect of the designed digital drive system under the two-phase flow condition, experiments under the gas-liquid two-phase flow condition were carried out on the water flow rig. In the experiments, 8-mm twin bent tubes were

Table 8 Driving system data from twin bent tubes with 8-mm inner diameter under the single-phase flow condition

Parameter	Average	Standard deviation	Repeatability (%)
Frequency of the driving signal (Hz)	205.554 271 7	0.001 55	0.000 75
Amplitude of the driving signal (%)	13.579 787 2	0.036 29	0.267 24
Amplitude of sensor A (%)	40.008 890 7	0.059 90	0.149 72
Phase of sensor A (°)	−0.106 780 75	0.027 68	
Amplitude of sensor B (%)	38.130 017 95	0.040 80	0.107 00
Phase of sensor B (°)	0.109 429 85	0.027 83	
Phase (°)	0.001 324 55	0.027 55	

Table 9 Driving system data from twin bent tubes with 25-mm inner diameter under the single-phase flow condition

Parameter	Average	Standard deviation	Repeatability (%)
Frequency of driving signal (Hz)	234.512 568	0.000 69	0.000 29
Amplitude of driving signal (%)	16.833 420 15	0.011 06	0.065 70
Amplitude of sensor A (%)	79.396 604 65	0.017 45	0.021 98
Phase of sensor A (°)	0.165 793	0.011 09	
Amplitude of sensor B (%)	79.990 237 45	0.016 14	0.020 18
Phase of sensor B (°)	−0.165 748 1	0.010 50	
Phase (°)	0.000 022 45	0.010 53	

connected to the fluid pipeline, and gas-liquid two-phase flow with a GVF of about 20% was constructed by a constant gas source. The data was recorded by the host computer. Fig. 8 shows the fluctuation of the driving signal frequency under the two-phase flow condition, and Fig. 9 shows the amplitude of the sensor signal under the two-phase flow condition.

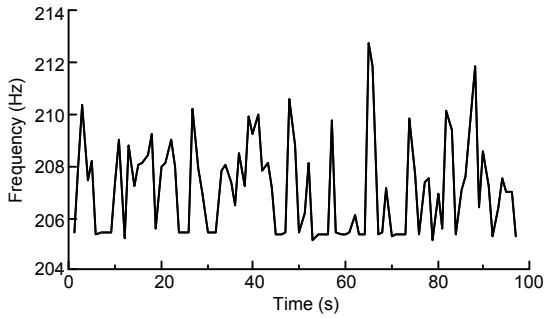

Fig. 8 Frequency of the driving signal under the two-phase flow condition

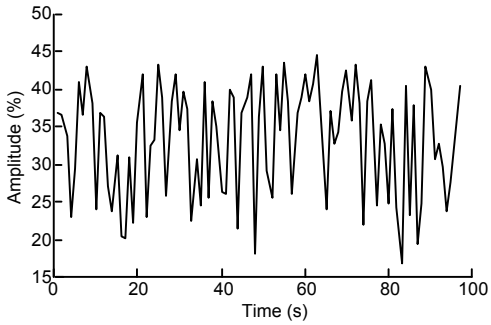

Fig. 9 Amplitude of the sensor signal under the two-phase flow condition

It can be seen from Table 8 that the twin bent tubes with an 8-mm inner diameter had a resonance frequency of 205.554 271 7 Hz under the single-phase flow condition. Fig. 8 shows the signal drive frequency fluctuation under the two-phase flow condition with a GVF of about 20%. The range was from 205 to 213 Hz. It basically conformed to the fluctuation of the resonance frequency under the two-phase flow condition.

Fig. 9 shows the sensor signal amplitude information under the two-phase flow condition. The amplitude was set to 40%. The amplitude of the sensor signal fluctuated between 20% and 43%, which basically conformed to the fluctuation of the signal amplitude of the Coriolis mass flowmeter under the two-phase flow condition. Under the two-phase flow condition, the converter designed in the study can drive the sensor to vibrate continuously.

Experiments were carried out on the unimproved Hilbert algorithm. Twin bent tubes with an 8-mm inner diameter were used as the primary instrument, which can measure a maximum flow point of 1000 kg/h. Under the single-phase flow condition, the Hilbert algorithm was verified on the water flow rig (Fig. 7) via the static start-stop method. Four kinds of flow points were selected for calibration, i.e., 160, 250, 420, and 600 kg/h. Each kind of flow point was measured three times.

Table 10 shows the calibration results of the unimproved and improved Hilbert algorithms under the single-phase flow condition. It can be seen from Table 10 that the unimproved Hilbert algorithm had larger errors and poorer repeatability. After adding the "dropout" technique and combining the FIR filter to improve the accuracy, the indication error was reduced and repeatability was significantly improved.

Another experiment was implemented based on the QD algorithm and the improved Hilbert algorithm. Experimental calibrations for single-phase flow and gas-water two-phase flow were carried out. The flow points were the same as in Table 10. Table 11 presents the calibration results of the QD and Hilbert algorithms under the single-phase flow condition.

The two-phase flow condition was created by adding gas to the pipe. Experiments under the two-phase flow condition were performed, and a constant gas source was added to the pipe at a gas flow rate of 600 mL/min. Table 12 shows the calibration results of the QD and Hilbert algorithms under the two-phase flow condition.

Under the single-phase flow condition, the indication error of the QD algorithm was smaller than that of the Hilbert algorithm at four kinds of flow points, and the repeatability was smaller than that of the Hilbert algorithm at most flow points. Host computer real-time data showed that the zero-point stability of the QD algorithm was better than that of the Hilbert algorithm. We can conclude that the QD algorithm is more robust under the single-phase flow condition.

Under the two-phase flow condition, due to the mixing of gas and liquid, the fluid density fluctuated, and the signal frequency and amplitude fluctuated wildly. Under a constant gas flow rate, as the flow rate of the liquid flow decreased, the GVF increased and

Table 10 Hilbert algorithm experimental calibration results

Flow point (kg/h)	Indication error (%)		Repeatability (%)	
	Unimproved Hilbert	Improved Hilbert	Unimproved Hilbert	Improved Hilbert
160	0.950	0.302	0.666	0.130
250	–0.045	–0.138	0.810	0.180
420	0.177	–0.085	0.370	0.085
600	–1.364	–0.080	0.082	0.023

Table 11 Experimental calibration results under the single-phase flow condition

Flow point (kg/h)	Indication error (%)		Repeatability (%)	
	QD	Hilbert	QD	Hilbert
160	0.111	0.302	0.049	0.130
250	–0.031	–0.138	0.139	0.180
420	–0.015	–0.085	0.066	0.085
600	–0.065	–0.080	0.038	0.023

Table 12 Experimental calibration results under the two-phase flow condition

Flow point (kg/h)	GVF (%)	Indication error (%)		Repeatability (%)	
		QD	Hilbert	QD	Hilbert
160	22.5	–6.228	–6.418	0.110	1.436
250	14.4	–3.917	–5.046	0.523	0.723
420	8.6	–2.102	–2.128	0.230	1.355
600	6.0	–1.820	–0.827	0.840	0.549

GVF: gas volume fraction

the indication errors of both algorithms increased. Only at the 600 kg/h flow point, were the indication error and repeatability of the Hilbert algorithm both smaller than the counterparts of the QD algorithm. When the gas content was large at the other three kinds of flow points, the error of the QD algorithm was smaller than that of the Hilbert algorithm, and the repeatability was larger than that of the Hilbert algorithm.

5 Conclusions

In this study, we have made improvements in the original Hilbert and DTFT algorithms and evaluated their performances on an embedded platform. Experiments have been carried out under single- and two-phase flow conditions to determine which algorithm has the smaller indication error.

The flow test results showed that the improved Hilbert algorithm can reduce the measurement error and improve repeatability. In the comparison experiment between the QD algorithm and the improved Hilbert algorithm, under the single-phase flow condition, the indication error of the QD algorithm was smaller than that of the Hilbert algorithm at four flow rates, and the repeatability was also smaller. Under the two-phase flow condition, the indication error of the QD algorithm was slightly smaller than that of the Hilbert algorithm at low flow rates, but the indication error of the Hilbert algorithm was smaller than that of the QD algorithm at the highest flow rate. A high-performance low-pass filter has been designed to improve the accuracy of the QD algorithm. The traditional DFT algorithm has been improved to greatly reduce the computational requirements and algorithm redundancy. The improved Hilbert algorithm reduced the influence of the endpoint effect of the algorithm, and the performances (accuracy and repeatability) were greatly improved compared with the unimproved algorithm.

Further research on signal processing methods is needed to provide diagnostic information to guarantee high accuracy of Coriolis mass flowmeters under complex field conditions. For example, an additional frequency can be excited to provide useful diagnostic parameters.

Contributors

Chunhui LI and Lijun SUN designed the research. Jiarong LIU and Haiyang LI processed the data. Chunhui LI drafted the manuscript. Jiarong LIU and Yang ZHANG helped organize the manuscript. Chunhui LI, Lijun SUN, and Huaxiang WANG revised and finalized the paper.

Acknowledgements

The authors would like to thank the technology support from both KROHNE UK and China. We would particularly like to acknowledge the discussion with Prof. Tao WANG from the University of Kent.

Compliance with ethics guidelines

Chunhui LI, Lijun SUN, Jiarong LIU, Yang ZHANG, Haiyang LI, and Huaxiang WANG declare that they have no conflict of interest.

References

Cage DR, 1988. Drive Means for Oscillating Flow Tubes of Parallel Path Coriolis Mass Flow Rate Meter. US Patent 473 814 4.

Carpenter BL, 1988. Ferromagnetic Drive and Velocity Sensors for a Coriolis Mass Flow Rate Meter. US Patent 477 783 3.

Fan LY, 1995. The description for staggered periodic sampling signal FIR filter in time and frequency domains. *Acta Electron Sin*, 23(9):70-74 (in Chinese).

Flecken P, 1989. Arrangement for Generating Natural Resonant Oscillations of a Mechanical Oscillating System. US Patent 480 189 7.

Huang DP, Wang JQ, Yu SD, et al., 2016. Research on the analog driving circuit of Coriolis mass flow meter. *Autom Instrum*, 31(1):71-76 (in Chinese). https://doi.org/10.19557/j.cnki.1001-9944.2016.01.018

Kalotay P, Bruck R, Emch A, et al., 1991. Flow Tube Drive Circuit Having a Bursty Output for Use in a Coriolis Meter. US Patent 500 910 9.

Kunze JW, Storm R, Wang T, 2014. Coriolis mass flow measurement with entrained gas. Proc Sensors and Measuring Systems, p.1-6.

Li M, Henry M, 2016. Signal processing methods for Coriolis mass flow metering in two-phase flow conditions. Proc IEEE Int Conf on Industrial Technology, p.690-695. https://doi.org/10.1109/icit.2016.7474833

Li M, Xu KJ, Hou QL, et al., 2010. Startup method of digital Coriolis mass flowmeter using alternating exciting of positive-negative step signal. *Chin J Sci Instrum*, 31(1):172-177 (in Chinese). https://doi.org/10.19650/j.cnki.cjsi.2010.01.030

Li XG, Xu KJ, 2009. Research on non-linear amplitude control method of Coriolis mass flow-tube. *J Electron Meas Instrum*, 23(6):82-86 (in Chinese).

Li Y, Xu KJ, Zhu ZH, et al., 2010. Study and implementation of processing method for time-varying signal of Coriolis mass flowmeter. *Chin J Sci Instrum*, 31(1):8-14 (in Chinese). https://doi.org/10.19650/j.cnki.cjsi.2010.01.002

Liu JR, Sun LJ, Wang HX, 2018. Signal processing of Coriolis mass flowmeters under gas-liquid two-phase flow conditions. Proc IEEE Int Instrumentation and Measurement Technology Conf, p.1-6. https://doi.org/10.1109/i2mtc.2018.8409623

Maginnis RL, 2003. Initialization Algorithm for Drive Control in a Coriolis Flowmeter. US Patent 650 513 5.

Mehendale A, 2008. Coriolis Mass Flow Rate Meters for Low Flows. PhD Thesis, University of Twente, Enschede, the Netherlands.

Meribout M, Saied IM, Hosani EA, 2018. A new FPGA-based terahertz imaging device for multiphase flow metering. *IEEE Trans Terahertz Sci Technol*, 8(4):418-426. https://doi.org/10.1109/TTHZ.2018.2824241

Meribout M, Shehaz F, Saied IM, et al., 2019. High gas void fraction flow measurement and imaging using a THz-based device. *IEEE Trans Terahertz Sci Technol*, 9(6): 659-668. https://doi.org/10.1109/TTHZ.2019.2945184

Röck H, Koschmieder F, 2009. Model-based phasor control of a Coriolis mass flow meter (CMFM) for the detection of drift in sensitivity and zero point. In: Mukhopadhyay SC, Gupta GS, Huang RY (Eds.), Recent Advances in Sensing Technology. Springer Berlin Heidelberg, p.221-240. https://doi.org/10.1007/978-3-642-00578-7_13

Romano P, 1990. Coriolis Mass Flow Rate Meter Having a Substantially Increased Noise Immunity. US Patent 493 419 6.

Shen TA, Tu YQ, Li M, et al., 2015. New sliding DTFT algorithm for phase difference measurement based on a new kind of windows and its analysis. *J Centr South Univ*, 46(4):1302-1309 (in Chinese). https://doi.org/10.11817/j.issn.1672-7207.2015.04.019

Shen TA, Li M, Li HN, et al., 2017. Phase difference estimation method for Coriolis mass flowmeter based on correlation and Hilbert transform. *Chin J Sci Instrum*, 38(12):2908-2914 (in Chinese).

Shimada H, 2013. Coriolis Flowmeter. US Patent 844 278 1.

Svete A, Kutin J, Bobovnik G, et al., 2015. Theoretical and experimental investigations of flow pulsation effects in Coriolis mass flowmeters. *J Sound Vibr*, 352:30-45. https://doi.org/10.1016/j.jsv.2015.05.014

Tao BB, Hou QL, Shi Y et al., 2014. Method and implementation of measuring the flow of liquid mixed with gas for Coriolis mass flowmeter. *Chin J Sci Instrum*, 35(8):1796-1802 (in Chinese). https://doi.org/10.19650/j.cnki.cjsi.2014.08.016

Tu YQ, Zhang HT, 2008. Method for CMF signal processing based on the recursive DTFT algorithm with negative frequency contribution. *IEEE Trans Inst Meas*, 57(11): 2647-2654. https://doi.org/10.1109/tim.2008.925006

Wang JH, 2013. Design of Coriolis Mass Flowmeter Based on Orthogonal Algorithm. MS Thesis, Shanghai Jiao Tong University, Shanghai, China (in Chinese).

Wang T, Baker R, 2014. Coriolis flowmeters: a review of

developments over the past 20 years, and an assessment of the state of the art and likely future directions. *Flow Meas Instrum*, 40:99-123. https://doi.org/10.1016/j.flowmeasinst.2014.08.015

Yang HY, Tu YQ, Zhang HT, et al., 2012. Phase difference measuring method based on SVD and Hilbert transform for Coriolis mass flowmeter. *Chin J Sci Instrum*, 33(9): 2101-2107 (in Chinese). https://doi.org/10.3969/j.issn.0254-3087.2012.09.026

Yang JW, Jia MP, 2006. Study on processing method and analysis of end problem of Hilbert-Huang spectrum. *J Vibr Eng*, 19(2):283-288 (in Chinese). https://doi.org/10.3969/j.issn.1004-4523.2006.02.025

Yokoi T, Owada H, 1996. Coriolis Type Mass Flowmeter Utilizing Phase Shifters for Phase Shifting of the Output Signals. US Patent 557 876 4.

Zamora M, Henry MP, 2008. An FPGA implementation of a digital Coriolis mass flow metering drive system. *IEEE Trans Ind Electron*, 55(7):2820-2831. https://doi.org/10.1109/TIE.2008.925646

Zhang JG, Xu KJ, Fang ZY, et al., 2017. Applications of digital signal processing technology in Coriolis mass flowmeter. *Chin J Sci Instrum*, 38(9):2087-2102 (in Chinese). https://doi.org/10.3969/j.issn.0254-3087.2017.09.001